Theoretical study of the reaction mechanism for the interaction of Si+ with disilane

Mohammad A. AlLaham and Krishnan Raghavachari

Citation: The Journal of Chemical Physics **95**, 2560 (1991); doi: 10.1063/1.460960
View online: http://dx.doi.org/10.1063/1.460960
View Table of Contents: http://scitation.aip.org/content/aip/journal/jcp/95/4?ver=pdfcov
Published by the AIP Publishing

Theoretical study of the reaction mechanism for the interaction of Si^+ with disilane

Mohammad A. Al-Laham and Krishnan Raghavachari
AT&T Bell Laboratories, Murray Hill, New Jersey 07974

(Received 19 February 1991; accepted 2 May 1991)

The reaction mechanism for the interaction of Si^+ with disilane has been studied by means of accurate *ab initio* molecular orbital techniques including polarized basis sets, effects of electron correlation, and zero-point corrections. There are two main accessible channels for the reaction, via Si^+ insertion into the Si–Si or the Si–H bonds. While both are exothermic and lead to the same products, the Si–Si insertion channel is the lower energy pathway. The insertion is followed by 1,2-H shift and H_2 elimination reactions. The reaction leads to the formation of two $Si_3H_4^+$ isomers, a noncyclic isomer, $H_3Si–SiH–Si^+$, and a cyclic isomer, $c(HSi–SiH_2–SiH)^+$, with no overall activation barriers. Formation of silane and $Si_2H_2^+$ is calculated to be significantly exothermic. Other fragmentation channels leading to the ions $Si_2H_5^+$, $Si_2H_4^+$, and $Si_2H_3^+$ are calculated to be endothermic. Our results are in good agreement with the available experimental results. We compare our results to those from previous studies of the interaction of Si^+ with silane and methylsilane.

I. INTRODUCTION

Chemical reactions of small silicon cluster ions with neutral molecules have been studied recently both experimentally[1–6] and theoretically.[7–9] Theoretical studies provide detailed mechanisms that can predict or explain experimental observations by eliminating reaction pathways with high-energy barriers from the many possible reaction channels. The results obtained from studying these reactions may be of special significance for processes such as those involved in silane chemical vapor deposition (CVD).[10–15]

In two previous studies, we have investigated the reaction mechanisms of the interaction of Si^+ with silane[7] and methylsilane.[8] In this work, we have undertaken a detailed *ab initio* molecular-orbital study of the reaction of Si^+ with disilane. Since disilane is an important species in silane plasmas, an understanding of such ion–molecule reactions is important to assess whether disilane plays a significant part in CVD mechanisms. In addition, these reactions present the novel possibility of the ion interacting with a silicon–silicon bond which was not present in the previous studies. Experimentally, Cheng, Yu, and Lampe have investigated the reactions of Si^+ with disilane by tandem and high-pressure mass spectroscopic techniques.[3] They have observed the formation of a variety of product ions, $Si_2H_n^+$ ($n = 1$–3,5) and $Si_3H_n^+$ ($n = 2$–4), although only $Si_2H_2^+$ and $Si_3H_4^+$ were formed by exothermic reaction channels. In this work, we have determined the reaction mechanisms for the different channels by means of a careful characterization of the relevant transition states, intermediates, and products.

II. THEORETICAL METHODS

The geometries of all the molecular species involved are determined by complete optimization at the Hartree–Fock (HF) level of theory[16] with the polarized 6-31G* basis set[17] (valence double-zeta *sp* with a set of *d*-type polarization functions on each Si atom). The geometries obtained at this level of theory are usually reliable[7] and can be used to perform single-point calculations with larger basis sets to yield relative energies.

For all the species considered in this study, the nature of the calculated stationary points was determined by analytical evaluation of the harmonic force constants and vibrational frequencies at the HF/6-31G* level.[18] All the minima are strictly characterized by the presence of all positive vibrational frequencies and all the transition states (TS) by the presence of one and only one imaginary vibrational frequency. To determine what minima a given transition state connects, we followed the intrinsic reaction coordinate[19] (IRC) in both the forward and reverse directions starting with the transition-state geometry. Zero-point energies (ZPE) are computed and included in the calculation of the relative energies for all species. The calculated 6-31G* zero-point energies are scaled by 0.9 to correct for the fact that the calculated frequencies at this level are typically too high by about 10%.[20]

Electron correlation effects are included by means of Møller–Plesset (MP) perturbation theory[21] with the 6-31G** basis set[17] (also including *p* functions on H). Complete fourth-order theory[22] (MP4) which has contributions from single, double, triple, and quadruple excitations from the starting HF determinant is used in all cases. Only the valence electrons are included in our correlation calculations.

Larger basis set effects may be important in this study,[9] particularly since there are many bond breakings and formations. The availability of partially broken bonds in transition-state structures makes these effects especially important. We have considered these basis set effects by performing single point calculations for all the species at the MP2 level of theory[23] using a large basis set, denoted as [6*s*,5*p*,2*d*,1*f*/3*s*,1*p*]. This basis set contains McLean and Chandler's contracted 6*s*,5*p* (Ref. 24) basis set on Si augmented with *d* and *f* polarization functions (Ref. 25), and a polarized triple-zeta basis set on H (Ref. 26). The additional energy lowerings due to the effect of larger basis sets are represented as Δ basis set in Tables I and III.

 0021-9606/91/162560-08$03.00

We use the unrestricted Hartree–Fock (UHF) method for all open-shells species in our calculations. The UHF wave functions of all the low-lying transition states and minima were tested for HF stability, and found to be stable. The UHF wave function is not an eigenfunction of the total spin (S^2) operator.[27] This causes contamination in the wave function from higher-spin contributions, making the calculated energy too high. The energy contributions from such contamination have been calculated at the spin-projected MP2 level[28] (PMP2/6-31G**) of theory. This ranges from 0–2 kcal/mol for most of the open-shell systems studied, and will be given as Δ spin in Tables I and III.

III. RESULTS AND DISCUSSION

The interaction of Si^+ with disilane proceeds via two reaction channels, the insertion into the Si–Si bond or into one of the Si–H bonds. The insertion into the Si–Si bond is the lower-energy channel, although the products from both channels can easily interconvert. The total and relative energies of all species involved in the reaction mechanism are listed in Table I. Table II lists the HF and MP2 energies with the larger basis set (contains f functions). In Tables I and II the transition states are denoted by odd numbers and the local minima by even numbers. Figure 1 represents the calculated reaction profile, including all reported stationary points on the potential energy surface. Tables III and IV, and Fig. 2 give the analogous results for the fragmentation products obtained from the cleavage of the Si–Si bonds from the local minima shown in Fig. 1.

The discussion in this reaction is divided into two parts. First we discuss the reaction mechanism of the Si–H insertion and the analogous results for the competitive Si–Si insertion. In the second part we discuss the fragmentation reactions resulting from Si–Si bond cleavage of the different intermediates. We compare our results with the experimental results[3] obtained by Cheng, Yu, and Lampe whenever appropriate.

IV. INSERTION MECHANISM

A. Si^+ insertion into the Si–H bond

Disilane, $H_3Si–SiH_3$ (A1), has D_{3d} symmetry and a $^1A_{1g}$ ground state. As shown below, the HF/6-31G* optimized Si–Si bond length is 2.353 Å and the Si–H bond length is 1.478 Å. These are in good agreement with the corresponding experimental values[29] of 2.327 and 1.486 Å.

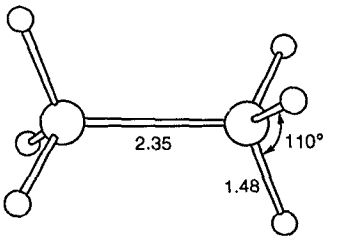

A1 (D_{3d})

The initial interaction of the Si^+ (^2P ground state) with the Si–H bond in disilane gives an ion–molecule complex, A2, with a binding energy of 30 kcal/mol. Similar binding energies were obtained in silane and methylsilane reactions.[7,8] The Si–H···Si interaction in the complex is almost linear (163°), with a H···Si interaction distance of 1.76 Å.

TABLE I. Total and relative energies (hartrees and kcal/mol) for the reaction of Si^+ with disilane.

Structure	Total energy (hartrees)[a] HF	MP2	MP3	MP4	ZPE[b] (kcal/mol)	Δ basis set[c] (kcal/mol)	PMP2-MP2[d] (kcal/mol)	Relative energy
A1, $H_3Si–SiH_3 + Si^+$	−869.864 87	−870.098 17	−870.146 09	−870.160 59	29.8	0.0	−0.7	0.0
A2, Complex	−869.899 94	−870.141 09	−870.188 96	−870.203 95	29.7	−2.8	−1.0	−30.4
A3, Si–H insertion TS	−869.876 34	−870.122 66	−870.171 15	−870.186 68	28.4	−8.0	−0.9	−26.0
A4, $H_3Si–SiH_2–SiH^+$	−869.916 39	−870.158 63	−870.204 02	−870.218 39	29.7	−5.2	−0.6	−41.5
A5, H migration TS	−869.905 02	−870.154 12	−870.198 99	−870.213 87	29.3	−7.0	−0.7	−40.9
A6, $H_3Si–SiH–SiH_2^+$	−869.936 34	−870.183 65	−870.228 84	−870.242 88	30.2	−6.5	−0.5	−57.5
A7, H migration TS	−869.907 99	−870.156 56	−870.201 56	−870.216 27	29.3	−7.3	−0.7	−42.7
A8, $H_3Si–Si–SiH_3^+$	−869.926 33	−870.166 63	−870.212 46	−870.226 62	30.4	−5.1	−0.5	−45.7
A9, Si–Si insertion TS	−869.863 69	−870.121 28	−870.169 19	−870.185 37	29.8	−12.7	−0.8	−28.3
A10, Complex	−869.899 04	−870.147 37	−870.194 90	−870.210 26	29.7	−7.4	−1.1	−39.1
A11, H_2 elimination TS	−869.844 94	−870.111 66	−870.157 41	−870.173 84	28.2	−9.0	−1.9	−20.1
A12, $H_3Si–SiH–Si^+ + H_2$	−869.871 27	−870.120 92	−870.169 72	−870.185 99	26.4	−3.8	−0.6	−23.0
A13, H_2 elimination TS	−869.831 28	−870.097 89	−870.141 87	−870.158 25	27.9	−9.1	−1.4	−10.2
A14, $H_3Si–Si–SiH^+ + H_2$	−869.856 11	−870.095 48	−870.142 86	−870.159 86	25.7	−2.8	−4.7	−10.4
A15, $c(H_2Si–SiH_2–H–SiH)^+$ TS	−869.913 25	−870.159 47	−870.204 66	−870.219 38	29.7	−7.6	−0.7	−44.6
A16, $c(H_2Si–SiH_2–H–SiH)^+$	−869.920 95	−870.174 67	−870.219 20	−870.233 96	30.7	−8.4	−0.6	−53.4
A17, H_2 elimination TS	−869.831 72	−870.104 55	−870.147 83	−870.163 80	28.8	−11.6	−0.7	−14.6
A18, $c(HSi–SiH_2–SiH)^+ + H_2$	−869.853 51	−870.117 01	−870.160 83	−870.177 03	26.1	−9.4	−0.7	−23.4

[a] Calculated with the 6-31G** basis set using HF/6-31G* geometries.
[b] Zero-point energies at the HF/6-31G* level scaled by 0.9.
[c] Larger basis set effects relative to the reactants $H_3Si–SiH_3 + Si^+$. Derived from MP2 calculations with a large [6s,5p,2d,1f/3s,1p] basis. See the text and Table II.
[d] Correction for spin contamination in the UHF wave function (see the text).

TABLE II. Total energies (hartrees) for the reaction of Si^+ with disilane using a large [6s,5p,2d,1f/3s,1p] basis set.

Structure	Total energy (hartrees)[a] HF	MP2
A1, H_3Si–SiH_3 + Si^+	−869.936 30	−870.222 05
A2, Complex	−869.972 71	−870.269 48
A3, Si–H insertion TS	−869.955 75	−870.259 22
A4, H_3Si–SiH_2–SiH^+	−869.990 79	−870.290 83
A5, H migration TS	−869.981 60	−870.289 17
A6, H_3Si–SiH–SiH_2^+	−870.013 46	−870.317 82
A7, H migration TS	−869.984 77	−870.292 04
A8, H_3Si–Si–SiH_3^+	−870.000 57	−870.298 65
A9, Si–Si insertion TS	−869.950 57	−870.265 34
A10, Complex	−869.976 01	−870.282 99
A11, H_2 elimination TS	−869.924 36	−870.249 85
A12, H_3Si–SiH–Si^+ + H_2	−869.946 58	−870.250 82
A13, H_2 elimination TS	−869.909 11	−870.236 32
A14, H_3Si–Si–SiH^+ + H_2	−869.930 24	−870.223 83
A15, $c(H_2Si$–SiH_2–H–$SiH)^+$ TS	−869.989 61	−870.295 40
A16, $c(H_2Si$–SiH_2–H–$SiH)^+$	−869.997 87	−870.311 90
A17, H_2 elimination TS	−869.910 03	−870.246 91
A18, $c(HSi$–SiH_2–$SiH)^+$ + H_2	−869.933 99	−870.255 80

[a] Calculated using HF/6-31G* geometries.

H···Si interaction in the complex is almost linear (163°), with a H···Si interaction distance of 1.76 Å.

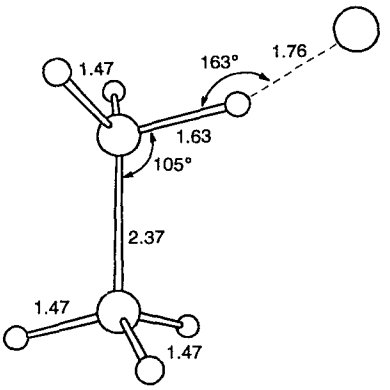

A2 (C_s)

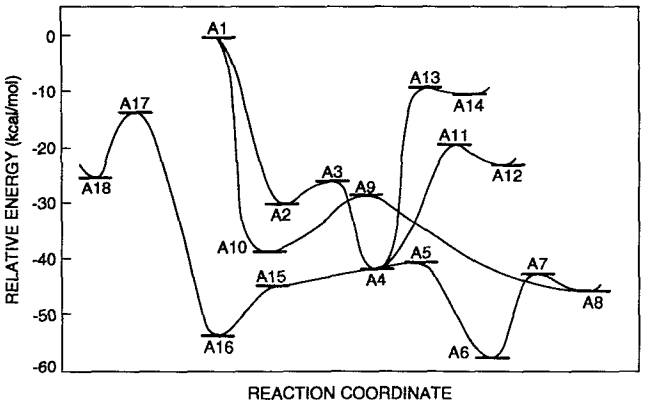

FIG. 1. Schematic energy profile for the interaction of Si^+ with disilane.

As expected, the structure of A2 is similar to the structures of silane and methylsilane complexes studied previously.[7,8] In fact, the silyl group in the methylsilane complex has almost the same geometry as the analogous silyl group in A2, indicating that the methyl group is a spectator at this mechanistic step.

Hydride transfer in A2 leads to SiH and $Si_2H_5^+$. However, the formation of these products is significantly endothermic as shown in a later section. The other possibility is the insertion of Si^+ into the Si–H bond for which the transition state A3 is shown. In A3 the newly forming Si–Si bond has a distance of 2.80 Å while the Si–H bond (1.54 Å) is almost completely formed.

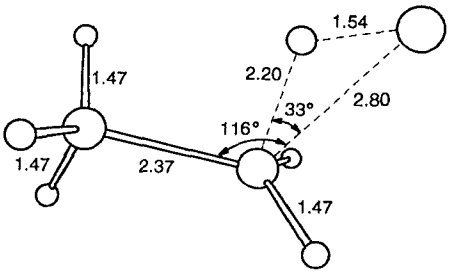

A3 (C_1)

The aforementioned transition state deviates form C_s symmetry by 22°. It lies 26 kcal/mol (Table I) below the separated species and has an energy barrier of only 4 kcal/mol from A2. Clearly, A3 is accessible in the reaction.

The insertion of the Si^+ into the Si–H bond yields H_3Si–SiH_2–SiH^+, shown as A4. A4 has a *gauche*-type conformation (the H–Si–Si–Si dihedral angle is roughly 60°) and no symmetry. The *trans* structure (C_s symmetry) is not a local minimum at the HF/6-31G* level of theory.[7] The geometry of A4 clearly indicates ionization of the σ lone pair on the terminal silicon.

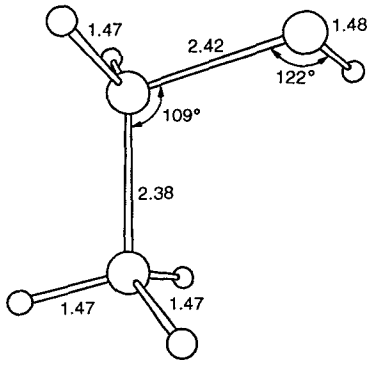

A4 (C_1)

The 122° Si–Si–H bond angle in A4 is similar to those seen previously[7,8] in H_3Si–SiH^+ and H_3C–SiH_2–SiH^+. The Si–H bond length in A4 is typical (1.46–1.47 Å) of Si–H bonds calculated at the HF/6-31G* level. A4 is more stable than A2 by more than 10 kcal/mol, as shown in Table I.

There are several possible channels for further reactions from A4. First we consider a H migration reaction across the

Si–Si bond. A5 is the transition state for the 1,2-H migration in A4. The structures of A5 and some other $Si_3H_6^+$ ions have been studied earlier (without including large basis set effects) as part of the sequential clustering reactions of Si^+ with silane.[7] The energy barrier of less than 1 kcal/mol calculated for A5 is similar to the low transition-state barrier reported[7] for the rearrangement of $H_3Si–SiH^+$ to the disilene ion ($H_2Si–SiH_2^+$).[7] In fact, this is typical of $R_2Si(H)–SiR^+$ and $R_2Si–Si(H)R^+$ rearrangement barriers. As shown in Table I, A5 is 41 kcal/mol below the separated reactants, and so it is easily accessible during the overall reaction.

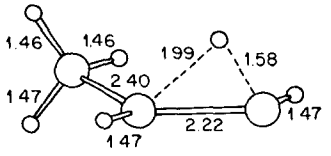

A5 (C_1)

The transition state above has no symmetry, and its structure reveals the nature of the partially broken and the newly formed bonds. The product of this 1,2-H shift is A6 ($H_3Si–SiH–SiH_2^+$). As reported in Table I, A6 is even more stable, lying 58 kcal/mol below the original reactants.

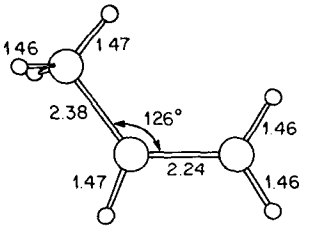

A6 (C_S)

The Si–Si bond length of 2.24 Å in A6 is similar to that (2.23 Å) found in the disilene ion[7] and $H_3C–SiH–SiH_2^+$.[8] A6 has C_s symmetry and a $^2A''$ ground state, indicating ionization from the Si–Si π bond.

A second 1,2-H migration is possible from A6, as shown in the transition state labeled A7:

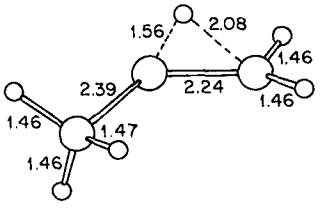

A7 (C_1)

The transition state A7 connects A6 to $H_3Si–Si–SiH_3^+$ (A8). A8 has a twisted C_2 structure, indicating significant deviation from a C_{2v} structure:

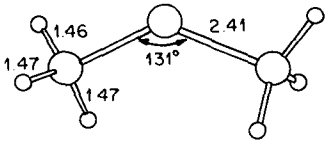

A8 (C_2)

Although A8 lies 46 kcal/mol below the starting reactants, it is less stable than A6 by 12 kcal/mol (Table I). As shown in Table I, A7 is slightly lower in energy than A5. Both H migration reactions have structures with low energies, making them easily accessible on the overall reaction potential energy surface.

B. Si^+ insertion into the Si–Si Bond

The second reaction channel occurs through Si^+ insertion into the Si–Si bond. This channel is more favorable than the Si–H insertion channel discussed earlier. The initial reaction starts by forming the ion–molecule complex A10, where Si^+ forms a complex with two hydrogens, one from each of the silyl groups.

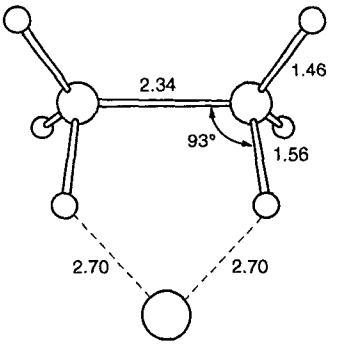

A10 (C_{2V})

A10 has C_{2v} symmetry, with long Si···H bonds (2.70 Å). For the two hydrogens close to the Si^+, the Si–H bond length is also elongated from 1.47 to 1.56 Å. The original Si–Si bond is unaffected by such complex formation, but the Si–Si–H angle is reduced form 110° in disilane to 93° in the complex. A10 is 39 kcal/mol below the starting reactants and 9 kcal/mol lower in energy than A2, as shown in Table I and Fig. 1.

The complex A10 leads to Si^+ insertion into the Si–Si bond to give A8 ($H_3Si–Si–SiH_3^+$) directly. A9 is the transition state for this insertion step.

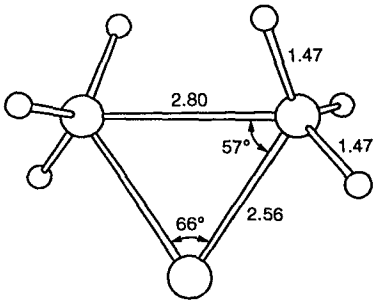

A9 (C_2)

In A9 the Si–Si distance between the silyl groups is 2.80 Å, 0.46 Å longer than that in disilane or in A10, and the newly formed Si–Si bonds are 2.56 Å in length. The two silyl groups in A9 are equivalent due to the C_2 symmetry of the molecule.

As shown, all stationary points on the reaction profile of the Si^+ insertion into both Si–Si and Si–H bonds in disilane are

exothermic. The Si–Si insertion channel, although lower in energy than the Si–H channel, does not lead to any new products. The existence of the Si–Si insertion channel can be attributed to the length (2.34 Å) and the comparative weakness of the Si–Si bond in disilane. The analogous C–Si insertion channel is not favorable in methylsilane (the C–Si bond length is 1.89 Å).

C. H_2 elimination

There are two possible $Si_3H_4^+$ isomers that can be obtained via H_2 elimination from A4, A6, or A8. There is a third cyclic $Si_3H_4^+$ isomer which can be formed by a different channel and it is considered later. The lowest energy transition state for an elimination of H_2 corresponds to A11:

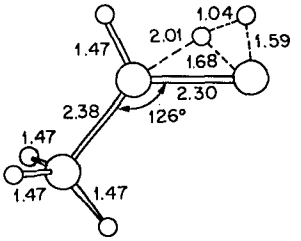

A11 (C_1)

The H···H distance in the transition state A11 is 1.04 Å, indicating that the H_2 bond is partially formed. The structure of A11 is similar to the structure of the transition state for the H_2 elimination in $H_3Si–SiH^+$.[7] The above 1,2-elimination transition state leads to A12 ($H_3Si–SiH–Si^+$). A12 has a $^2A''$ ground state, corresponding to ionization from the Si–Si π orbital. Again, the structures of A12 and the analogous $H_3C–SiH–Si^+$ are similar,[8] except for a slightly larger Si–Si–Si bond angle in the former compared with C–Si–Si bond angle in the latter.

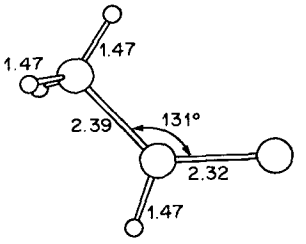

A12 (C_S)

Table I indicates that A12 lies 23 kcal/mol below the starting reactants, making it a major product of the reaction, in agreement with the experimental observation of $Si_3H_4^+$ by Cheng, Yu, and Lampe.[3]

The second H_2 elimination pathway has the transition state A13. The barrier for A13 is 9 kcal/mol *higher* (Table I) than the transition state A11, but still 10 kcal/mol below the starting reactants.

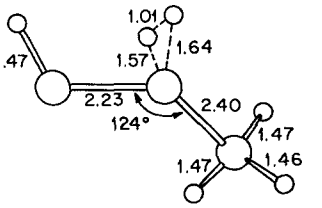

A13 (C_1)

The structure of A13 shows a H···H bond length of 1.01 Å, again indicating partial formation of a H_2 bond. The elimination of H_2 yields $H_3Si–Si–SiH^+$ (A14), which has no symmetry and proceeds with no barrier. Table I and Fig. 1 indicate that A14 is less stable than its isomeric form A12 by 13 kcal/mol. It is likely that A14, if formed, will rearrange rapidly to A12 with a low-energy barrier. The structures of A14 and the analogous $H_3C–Si–SiH^+$ are similar except for the Si–Si–Si bond angle which is 10° larger than the corresponding C–Si–Si bond angle.[8]

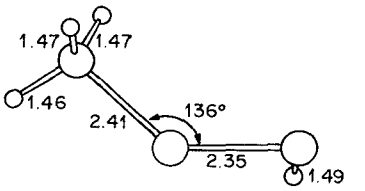

A14 (C_1)

Among all open-shell systems presented, A14 is the only system where there is a large spin contamination in the UHF wave function. This is probably related to the unusual nature of the terminal Si–H unit where the hydrogen shows an incipient tendency to bridging. Spin projection reveals an energy contribution of about 5 kcal/mol, compared with the rest of the open-shell systems where such corrections range from 0–2 kcal/mol.

D. Formation of hydrogen-bridged isomer

The next possible pathway from $H_3Si–SiH_2–SiH^+$ (A4) leads to a novel but very stable hydrogen-bridged isomer. The transition state leading to this hydrogen-bridged structure is given as

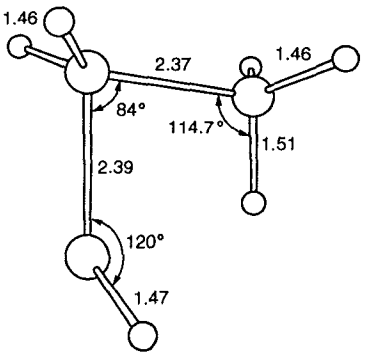

A15 (C_1)

The Si–H bond length for the bridging hydrogen in A15 is stretched to 1.51 Å and the Si–Si–Si bond angle is reduced from 109° to 84°.

The transition state A15 connects $H_3Si–SiH_2–SiH^+$ and A16, an unusual cyclic hydrogen bridged structure $c(H_2Si–SiH_2–H–SiH)^+$. As shown below, A16 has two typical Si–Si bonds and two long Si–H bonds (1.66 and 1.68 Å). The Si–Si–Si bond angle is 72° and the bridging Si–H–Si angle is 111°. The Si–Si distance between the two silicons attached to the bridging hydrogen is only 2.75 Å, perhaps indicative of a weak interaction. A16 lies 53 kcal/mol below the starting reactants and is only 4 kcal/mol less stable than A6, the most stable structure studied (Table I). This bridging energy in A16 is large enough to overcome the strain involved in the formation of a four membered ring. A similar structure was reported for $Si_3H_7^+$ in the study of the clustering reactions of SiH_3^+ with silane.[9]

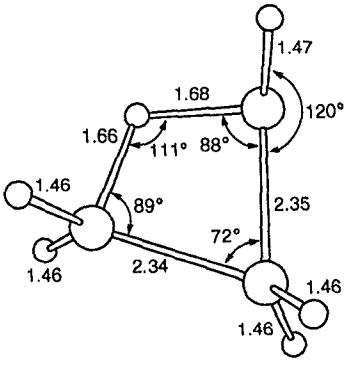

A16 (C_1)

At the HF/6-31G* level of theory, A15 has a 2 kcal/mol energy barrier from A4. However, including the correlation energy at the MP4/6-31G** level favors the transition state making A15 3 kcal/mol *lower* in energy than A4, as shown in Table I. This clearly indicates that the barrier to lead to the cyclic structure A16 is very small. Geometry optimization at levels that include electron correlation effects will be necessary to give a more reliable estimate of this energy barrier.

E. Cyclic product formation

The bridged structure can lead to cyclic $Si_3H_4^+$ through H_2 elimination. The transition state for this step is given as A17. As shown, A16 loses the bridging hydrogen with one of the adjacent hydrogens to form H_2. In A17 the H–H distance is 0.99 Å, indicating bond formation, and the Si···H distances are 1.59 Å, indicating bond breaking. A17 is 39 kcal/mol higher in energy than A16 but 15 kcal/mol *lower* in energy than the starting reactants, as shown in Table I and Fig. 1.

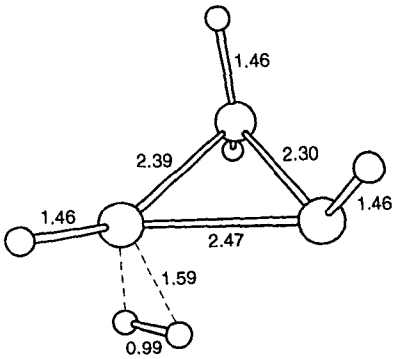

A17 (C_1)

The elimination of H_2 from A16 through the transition state A17 leads to $c(HSi–SiH_2–SiH)^+$ (A18), the silicon analogue of cyclopropene cation. As shown, A18 has C_{2v} symmetry. Partial double-bonded Si–Si has a distance of 2.19 Å, while the other Si–Si bond distance is 2.35 Å. A18 lies 23 kcal/mol below the starting reactants, making it one of the stable products of the reaction. It is interesting to note that the cyclic isomer A18 is comparable in stability to the other major product, A12. However, the barrier to lead to A12 is slightly lower in energy than the one leading to A18. Nevertheless, since both barriers are substantially lower than the separated species, it is

TABLE III. Total and relative energies (hartrees and kcal/mol) for the fragmentation products of the reaction of Si^+ with disilane.

Structure	Total energy (hartrees)[a] HF	MP2	MP3	MP4	ZPE[b] (kcal/mol)	Δ basis set[c] (kcal/mol)	PMP2–MP2[d] (kcal/mol)	Relative energy
B1, $H_3Si–SiH_2 + SiH^+$	−869.836 05	−870.070 27	−870.118 84	−870.133 76	27.1	−1.3	−0.5	+13.0
B2, $H_3Si–SiH_2^+ + SiH$	−869.848 65	−870.077 65	−870.125 44	−870.139 86	27.3	−2.3	−0.8	+8.1
B3, $H_3Si–SiH + SiH_2^+$	−869.799 18	−870.030 04	−870.077 04	−870.091 63	26.3	−3.3	0.0	+37.2
B4, $H_3Si–SiH^+ + SiH_2$	−869.827 18	−870.056 77	−870.105 03	−870.119 89	26.2	−2.9	−0.5	+19.2
B5, $H_2Si–SiH_2^+ + SiH_2$	−869.839 31	−870.075 46	−870.123 55	−870.138 32	26.3	−5.0	−0.5	+5.7
B6, $H_3Si–Si + SiH_3^+$	−869.830 02	−870.060 64	−870.107 98	−870.122 29	28.1	−2.1	−0.8	+20.1
B7, $H_3Si–Si^+ + SiH_3$	−869.841 86	−870.074 78	−870.123 64	−870.138 79	27.7	−2.6	−0.3	+9.4
B8, $H_2Si(H)Si^+ + SiH_3$	−869.834 02	−870.078 23	−870.126 95	−870.142 57	26.8	−4.2	−0.3	+4.5
B9, $HSi(H_2)Si^+ + SiH_3$	−869.818 36	−870.077 89	−870.125 16	−870.141 90	26.7	−7.4	−0.3	+1.6
B10, $Si(H_3)Si^+ + SiH_3$	−869.834 26	−870.095 10	−870.144 59	−870.161 26	28.4	−7.1	−0.3	−8.5

[a] Calculated with the 6-31G** basis set using HF/6-31G* geometries.
[b] Zero-point energies at the HF/6-31G* level scaled by 0.9.
[c] Larger basis set effects relative to the reactants $H_2Si–SiH_2^+$ and SiH_4. Derived from MP2 calculations with a large [6s,5p,2d,1f/3s,1p] basis. See the text and Table IV.
[d] Correction for spin contamination in the UHF wave function (see the text).

likely that both cyclic and noncyclic products are formed in this reaction.

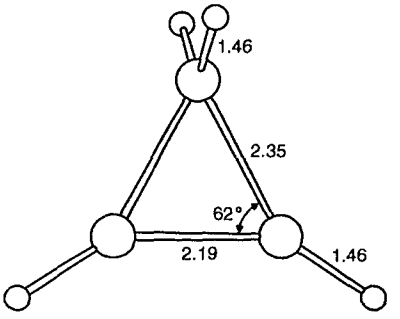

A18 (C_{2v})

We did not study the additional reactions involving a second H_2 elimination from A12 or A14 in detail. Preliminary investigation revealed that one of the possible products of such a reaction, $c(Si\text{–}SiH_2\text{–}Si)^+$, is lower in energy than the starting reactant by 14 kcal/mol. Additional calculations are needed for better understanding of the feasibility of further reactions from both A12 and A14.

V. FRAGMENTATION PRODUCTS

Apart from the elimination of H_2, there are several other possible fragmentation channels which can lead to a variety of other products. One of the obvious possible products is the formation of $SiH_4 + Si_2H_2^+$. There are two stable isomers of the $Si_2H_2^+$ ion, a bridged form, $Si(H_2)Si^+$, which has a $^2A_1$ ground state, and a nonbridged form $H_2Si\text{–}Si^+$ with a $^2B_1$ ground state. The overall reaction energy for the formation $H_2Si\text{–}Si^+$ and silane is exothermic by 14 kcal/mol. In a previous paper,[7] the reverse reaction of $H_2Si\text{–}Si^+ + SiH_4$ has been studied in detail and leads to $Si_3H_6^+$ isomers such as A4 and A6 without any overall activation barrier. Thus the forward reaction of Si^+ with Si_2H_6 will clearly lead to the formation of $H_2Si\text{–}Si^+$. The formation of the bridged $Si(H_2)Si^+$ ion $+ SiH_4$ is exothermic by 21 kcal/mol, but requires the rearrangement of the $H_2Si\text{–}Si^+$ ion. Experimentally, the reaction of Si^+ with disilane leading to $Si_2H_2^+ + SiH_4$ has been identified to be exothermic by $\simeq 18$ kcal/mol.[3]

There are several other reactions products which can all be obtained by simple bond cleavage reactions form the local minima on the reaction surface. We studied the Si–Si bond cleavage reactions in A4, A6, and A8. The total and relative energies of the fragments studied are given in Table III, and the effect of using the [6*s*,5*p*,2*d*,1*f*/3*s*,1*p*] basis set is given in Table IV. Figure 2 shows a schematic representation of the relative energies of the fragments.

The bond cleavage reactions of one of the Si–Si bonds in A4 ($H_3Si\text{–}SiH_2\text{–}SiH^+$) can lead to $H_3Si\text{–}SiH_2 + SiH^+$ (B1) or $H_3Si\text{–}SiH_2^+ + SiH$ (B2). As shown in Fig. 2 and Table III, both are endothermic reactions. The cleavage of the other Si–Si bond leads to B8, $H_3Si + H_2Si(H)Si^+$ ($H_2Si\text{–}SiH^+$ rearranges without a barrier to the bridged isomer),[30] which is endothermic by 5 kcal/mol.

Three other products can be obtained from one of the Si–Si bond cleavage of A6 ($H_3Si\text{–}SiH\text{–}SiH_2^+$). The fragmentation reaction leading to B3 ($H_3Si\text{–}SiH + SiH_2^+$) is endothermic by 37 kcal/mol, as shown in Table III. The other reaction channel, which leads to B4 ($H_3Si\text{–}SiH^+ + SiH_2$) is also endothermic, but it is 18 kcal/mol lower in energy than B3. B4 can rearrange to its isomeric form $H_2Si\text{–}SiH_2^+ + SiH_2$, labeled B5 in Tables III and IV. The overall reaction leading to this isomer is also endothermic by about 6 kcal/mol (Table III). It is clear that the above Si–Si bond cleavage reactions of A6 are all endothermic, and can be formed only in the presence of excess energy.

The last studied fragmentation products are those obtained from the Si–Si bond cleavage in A8 ($H_3Si\text{–}Si\text{–}SiH_3^+$). B6 ($H_3Si\text{–}Si + SiH_3^+$) is a possible reaction fragment of A8. As the relative energies in Table III indicate, the reaction leading to B6 is endothermic by 20 kcal/mol. The other fragment considered is $H_3Si\text{–}Si^+ + SiH_3$ (B7). Again, B7 can be obtained by an overall endothermic process of 9 kcal/mol (Table III). B7 can rearrange to $H_2Si(H)Si^+ + SiH_3$, $HSi(H_2)Si^+ + SiH_3$, or $Si(H_3)Si^+ + SiH_3$, represented as B8, B9, or B10, respectively.[30] As shown in Table III, both B8 and B9 are produced by an overall endothermic reactions (5

TABLE IV. Total energies (hartrees) for the fragmentation products of the reaction of Si^+ with disilane using a large [6*s*,5*p*,2*d*,1*f*/3*s*,1*p*] basis set.

Structure	Total energy (hartrees)[a] HF	MP2
B1, $H_3Si\text{–}SiH_2 + SiH^+$	−869.908 55	−870.196 21
B2, $H_3Si\text{–}SiH_2^+ + SiH$	−869.921 74	−870.205 14
B3, $H_3Si\text{–}SiH + SiH_2^+$	−869.872 31	−870.159 13
B4, $H_3Si\text{–}SiH^+ + SiH_2$	−869.900 55	−870.185 25
B5, $H_2Si\text{–}SiH_2^+ + SiH_2$	−869.916 75	−870.207 29
B6, $H_3Si\text{–}Si + SiH_3^+$	−869.901 93	−870.187 85
B7, $H_3Si\text{–}Si^+ + SiH_3$	−869.916 21	−870.202 82
B8, $H_2Si(H)Si^+ + SiH_3$	−869.911 68	−870.208 79
B9, $HSi(H_2)Si^+ + SiH_3$	−869.898 79	−870.213 56
B10, $Si(H_3)Si^+ + SiH_3$	−869.916 19	−870.230 34

[a] Calculated using HF/6-31G* geometries.

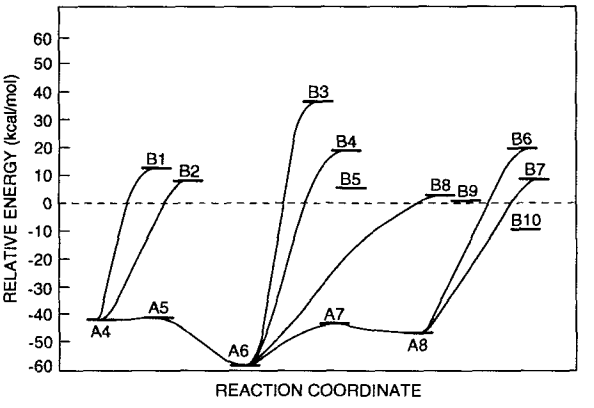

FIG. 2. Schematic representation of the relative energies of the fragments obtained from the Si–Si bond cleavage of the local minima in Fig. 1. The transition states for the rearrangement of some of the species are not presented.

and 2 kcal/mol, respectively). On the other hand, the isomer B10 can be obtained by an overall exothermic reaction of 9 kcal/mol, as shown in Table III and Fig. 2. However, since B7 itself is endothermic by 9 kcal/mol, rearrangements leading to B8, B9, and B10 are unlikely under low-energy experimental conditions.

As shown in Table III and Fig. 2, having the positive charge on the larger fragments of the Si–Si bond cleavage reactions is more favorable due to the stabilization effect resulting from charge delocalization. The energy lowering can be as large as 18 kcal/mol, as shown when comparing the relative energies of B3 and B4. The calculated energy difference between B6 and B7 is 11 kcal/mol and only 5 kcal/mol between B1 and B2, as shown in Table III.

VI. COMPARISON WITH INSERTION REACTIONS IN SILANE AND METHYLSILANE

The similarities in the structures of the stationary points on the reaction profiles of the Si^+ insertion into the Si–H bonds in silane, methylsilane and disilane suggests that the mechanism is localized to the vicinity of the attacked silyl group. Considering only the Si–H insertion channel, methylsilane and disilane can be considered as methyl or silyl substituted SiH_4, respectively.

The difference in mechanism between methylsilane and disilane interactions with Si^+ arises when comparing the insertion of Si^+ into the C–Si and the Si–Si bonds. In disilane, the Si^+ insertion into the Si–Si bond is the lower energy channel, as discussed earlier. In methylsilane,[8] the transition state for Si^+ insertion into the C–Si bond has an energy which is only 6 kcal/mol below the starting reactants. On the other hand, for the Si–H insertion channel in methylsilane, the analogous transition state is 19 kcal/mol lower than the starting materials.[8] This indicates that the C–Si insertion channel is not the favorable path in the interaction between Si^+ and methylsilane.

Comparison of the simple Si–Si bond cleavage in disilane and methylsilane reactions shows some difference. While in methylsilane bond cleavage of H_3C–Si–SiH_3^+ leading to the fragments H_3C–Si^+ and SiH_3 is clearly exothermic. In disilane, the analogous reaction is endothermic.

VII. CONCLUSIONS

Accurate theoretical calculations have been performed to study the interaction of Si^+ with disilane. In good agreement with the experimental results, we calculate two exothermic reactions. The first gives silane and $Si_2H_2^+$, while the other gives $Si_3H_4^+$ and H_2. Both noncyclic and cyclic $Si_3H_4^+$ isomers can be formed. In the initial interaction, the Si^+ inserts into the Si–Si bond or the Si–H bond, with the former being lower in energy. When proceeding via the Si–H insertion channel, the interaction of Si^+ with disilane has a similar reaction profile to those for the interactions with methylsilane or silane. This leads to the conclusion that the mechanism of the Si–H insertion is localized, and that it is possible to study insertion reaction mechanisms in larger substituted silane systems by restricting the calculations to the relevant part of the molecule. The use of large basis sets that include *d*- and *f*-basis functions is important to reach definitive conclusions in mechanistic studies.

[1] T-Y. Yu, T. M. H. Cheng, V. Kempten, and F. W. Lampe, J. Phys. Chem. **76**, 3321 (1972).
[2] J. M. S. Henis, G. W. Stewart, M. K. Tripodi, and P. P. Gaspar, J. Chem. Phys. **57**, 389 (1972).
[3] T. M. H. Cheng, T-Y. Yu, and F. W. Lampe, J. Phys. Chem. **78**, 1184 (1974).
[4] B. H. Boo and P. B. Armentrout, J. Am. Chem. Soc. **109**, 3549 (1987).
[5] M. L. Mandich, W. D. Reents, and M. F. Jarrold, J. Chem. Phys. **88**, 1703 (1988).
[6] M. L. Mandich and W. D. Reents and K. Kolenbrander, J. Chem. Phys. **92**, 437 (1989).
[7] K. Raghavachari, J. Chem. Phys. **88**, 1688 (1988).
[8] K. Raghavachari, J. Phys. Chem. **92**, 6284 (1988).
[9] K. Raghavachari, J. Chem. Phys. **92**, 452 (1990).
[10] M. E. Coltrin, R. J. Lee, and J. A. Miller, J. Electrochem. Soc. **131**, 425 (1984).
[11] H. Chatham and A. J. Gallagher, J. Appl. Phys. **58**, 159 (1985).
[12] C. A. DeJoseph, P. D. Haaland, and A. Garscadden, IEEE Trans. Plasma Soc. PS-**14**, 165 (1986).
[13] J. M. Jasinski, B. S. Meyerson, and B. A. Scott, Ann. Rev. Phys. Chem. **38**, 109 (1987).
[14] M. J. Kushner, J. Appl. Phys. **63**, 2532 (1988).
[15] S. Veprek and M. Heintze, Plasma Chem. Plasma Proc. **10**, 3 (1990).
[16] For a general introduction to Hartree–Fock based methods, see, W. J. Hehre, L. Radom, P. v. R. Schleyer, and J. A. Pople, *Ab Initio Molecular Orbital Theory* (Wiley, New York, 1986).
[17] P. C. Hariharan and J. A. Pople, Chem. Phys. Lett. **66**, 217 (1972); M. M. Francl, W. J. Pietro, W. J. Hehre, J. S. Binkley, M. S. Gordon, D. J. DeFrees, and J. A. Pople, J. Chem. Phys. **77**, 3654 (1982).
[18] J. A. Pople, R. Krishnan, H. B. Schlegel, and J. S. Binkley, Int. J. Quant. Chem. Symp. **13**, 255 (1979).
[19] C. Gonzalez and H. B. Schlegel, J. Chem. Phys. **90**, 2154 (1989).
[20] J. A. Pople, H. B. Schlegel, R. Krishnan, D. J. DeFrees, J. S. Binkley, M. J. Frisch, R. A. Whiteside, R. F. Hout, and W. J. Hehre, Int. J. Quant. Chem. Symp. **15**, 269 (1981).
[21] C. Møller and M. S. Plesset, Phys. Rev. **46**, 618 (1934).
[22] R. Krishnan, M. J. Frisch, and J. A. Pople, J. Chem. Phys. **72**, 4244 (1980), and references cited therein.
[23] J. S. Binkley and J. A. Pople, Int. J. Quant. Chem. **9**, 229 (1975).
[24] A. D. McLean and G. S. Chandler, J. Chem. Phys. **72**, 5639 (1980).
[25] The 2*d* exponents used are 0.9 and 0.225; the *f* exponent is 0.32.
[26] R. Krishnan, J. S. Binkley, R. Seeger, and J. A. Pople, J. Chem. Phys. **72**, 650 (1980).
[27] P.-O. Löwdin, Phys. Rev. **97**, 1509 (1955).
[28] H. B. Schlegel, J. Chem. Phys. **84**, 4530 (1986), and references therein.
[29] J. H. Callomon, E. Hirota, K. Kuchitsu, W. J. Lafferty, A. G. Maki, and C. S. Pote, in *Structure Data on Free Polyatomic Molecules*, edited by K. H. Hellwege and A. M. Hellwege (Springer, Berlin, 1976).
[30] B. T. Colegrove and H. F. Schafer, J. Chem. Phys. **93**, 7230 (1990).